Input Current Control of Boost Converters using Current-Mode Controller Integrated with Linear Quadratic Regulator

M.A. Abdullah*, C.W. Tan*, A.H.M. Yatim*, M.R.D. Al-Mothafar**, S.M. Radaideh**

*Department of Energy Conversion, Faculty of Electrical Engineering, Universiti Teknologi Malaysia (UTM), 81300 Skudai, Johor, Malaysia.

**Electrical Engineering Department, Faculty of Engineering, Jordan University of Science and Technology (JUST), 22110 Irbid, Jordan

‡Corresponding Author; M.A. Abdullah,Department of Energy Conversion, Faculty of Electrical Engineering, Universiti Teknologi Malaysia (UTM), 81300 Skudai, Johor, Malaysia, +60107059835, aaamajid@live.utm.my, cheewei@fke.utm.my, halim@ieee.org, mothafar@just.edu.jo, srad@just.edu.jo

Received: 22.02.2012 Accepted:19.03.2012

Abstract- The application of power electronic converters in the renewable energy systems significantly increases their efficiencies by maintaining the operation of these systems at the optimal operating points, therefore, absorbing the maximum available power from the renewable sources all the time. In this paper, the small-signal models of the open-loop, current-mode controlled boost converter are derived. In addition, both the Current Mode Control (CMC) and the Linear Quadratic Regulator (LQR) methods are combined to design a controller that forces the input current of the converter to follow accurately a reference current, which could be generated using maximum power point tracking (MPPT) algorithms. The controller performance is tested under transient conditions and with disturbance signals using MATLAB/Simulink simulation package. The simulation results indicate that both a good response and disturbance rejection are achieved in tested conditions.

Keywords- Boost converter; Peak current mode control; Linear quadratic regulator; Renewable energy.

1. Introduction

Renewable energy sources have gained extensive interest in the newly published research papers during the recent years. This is significantly due to a large extent, to conventional sources having harmful impacts on the environment. They are also expected to deplete in the near future. On the contrary, sustainable sources are found to be clean, pollution-free, inexhaustible and secure [1]. However, these environmentally friendly sources are instantaneously varying and the power that can be extracted is changeable. Therefore, a controller has to be included in the renewable energy systems to maintain producing the maximum power of these sources at all times.

In the renewable energy conversion systems, the optimal operating points, at which the system produces the maximum power, are constantly varying; due the intermittent nature of the environmental conditions, such as: the wind speed in the wind energy conversion system, and the temperature and the irradiance in the photovoltaic system. Similarly, depending on the application, load characteristics may also greatly vary. Consequently, there is a need to a converter circuit that effectively matches source and load impedances dynamically, in order to extract maximum power at any given instant [2-3].

Matching the source and the load impedances could be achieved by adjusting the duty-cycle of the converter that interfaces them. To determine the optimal duty cycle, there are many available algorithms, referred to as maximum power point tracking (MPPT) algorithms. The many different techniques for MPPT of photovoltaic and wind energy conversion systems have been reviewed and discussed deeply in [1, 4-5]. Examples of the available MPPT algorithms are: perturbation of any of converter variables, namely: the input current [6], the input voltage [7], or the

duty-cycle [8-10], and monitors the resulted change in the input power of the converter.

Current-mode control (CMC) is one of the feedback control techniques used for the power electronic converters by which the switch is controlled to be opened at the peaks of the inductor current and closed at a programmed level of the current. It consists of two distinctive loops; namely the inner loop and the outer loop. The inner loop combines all the state variables of the converter multiplied by different gains, whereas the outer loop can be modified according to the variable that needs to be controlled. There are many methods used to apply current mode control, such as peak-current mode control (PCMC) [11], average current mode control [12] and sensorless current mode control [13]. Some of the advantages of the CMC are the automatic input line feed-forward, and the inherent cycle-by-cycle overload protection.

Classical feedback control techniques are usually used for controlling boost DC-DC converters. However, there have been several attempts to control DC-DC converters using the linear quadratic regulator (LQR) technique that guarantees obtaining the desired optimal performance [14]. In addition, it does not depend on the system order, and is intrinsically stable. Many researchers in the past few years used the LQR method to control their systems. Nonetheless, almost all of them focused on regulating the output voltage. Studies [15-20] apply the LQR technique with integral actions to different DC-DC converters systems. The simulation and experimental results of these studies show very good performance of the systems under transient conditions and with disturbances. The weights in the controlling matrices Q and R of the LQR are user defined. However, they are achieved by genetic algorithm in [21-22] .

This paper aims to design a controller on the basis of the CMC and LQR. The outer loop of the CMC is modified to include the feedback gains of the LQR. The desired objective of the controller is to force the inductor current of the boost converter to follow accurately a given reference current; which in fact could be the output of the MPPT algorithms.

In the subsequent sections, the modeling of the converter is described and the model is then augmented to include the LQR feedback gains. Following this, the simulation results are shown and discussed and finally, a conclusion is drawn.

2. Boost Converter Modeling

As shown in Fig. 1, the boost converter circuit consists of four components: inductor, electronic switch; diode and output capacitor [23]. The converter has two modes of operation; namely the continuous and discontinuous conduction mode (CCM and DCM). In CCM, currently used in this study, the inductor current is always greater than zero. In contrast, it is zero for some time of the period T_s in DCM.

The switching of the converter occurs at a constant frequency f_s . The on-time interval is DT_s , and the off-time interval is $D'T_s$. Where D is the duty ratio of the switch and D' is $(1-D)$. The circuit in Fig.1 can be redrawn for the on and off intervals as in Fig.2 (a) and (b), respectively.

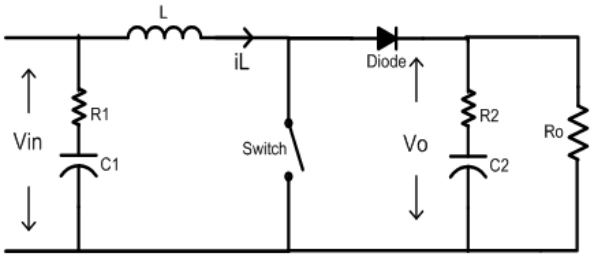

Fig. 1. Boost converter circuit topology.

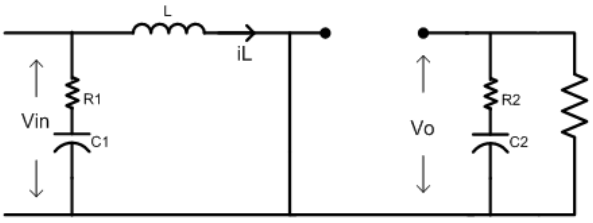

(a)

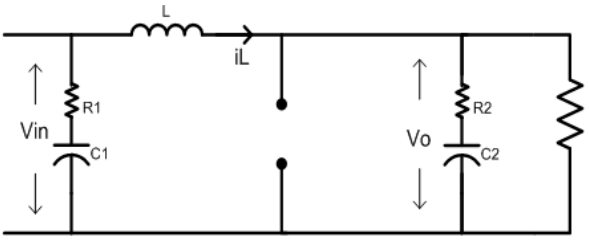

(b)

Fig. 2. (a) The first interval when the switch is on (closed), (b) The second interval when the switch is off (opened).

In this section, the small signal models of the open loop converter, as well as the CMC are derived.

2.1. Modeling of the Open-Loop Converter

Boost converter, by its nature, is a nonlinear system. To present it in a linear form, the state space averaging method is used to approximate it to a continuous nonlinear system, and the linearization is used to approximate the resulted nonlinear system to a linear one [24]. For the control purposes, a current source is added at the output of the converter to represent a load disturbance in the model. The first step in the state space averaging method is the forming of the state equations that describe the first and second intervals, which are represented as (1) and (2), respectively.

$$\dot{\mathbf{X}} = \mathbf{A_{ON}}\mathbf{X} + \mathbf{B_{ON}}\mathbf{U} \tag{1}$$

$$v_o = C_{ON}X + E_{ON}U \tag{2}$$

$$\dot{\mathbf{X}} = \mathbf{A_{OFF}}\mathbf{X} + \mathbf{B_{OFF}}\mathbf{U} \tag{3}$$

$$v_o = C_{OFF}X + E_{OFF}U \tag{4}$$

Where:

$$\mathbf{X} = \begin{bmatrix} i_L & v_{c1} & v_{c2} \end{bmatrix}', \qquad U = \begin{bmatrix} V_{in} & I_{in} \end{bmatrix}' \tag{5}$$

$$A_{ON}=\begin{bmatrix} 0 & 0 & 0 \\ 0 & \frac{-1}{R_1C_1} & 0 \\ 0 & 0 & \frac{-1}{(R_2+R_o)C_2} \end{bmatrix} \quad (6)$$

$$B_{ON}=\begin{bmatrix} \frac{1}{L} & 0 \\ \frac{1}{R_1C_1} & 0 \\ 0 & \frac{R_o}{(R_2+R_o)C_2} \end{bmatrix} \quad (7)$$

$$C_{ON}=\begin{bmatrix} 0 & 0 & \frac{R_o}{R_o+R_2} \end{bmatrix} \quad (8)$$

$$E_{ON}=\begin{bmatrix} 0 & \frac{R_2R_o}{R_o+R_2} \end{bmatrix} \quad (9)$$

$$A_{OFF}=\begin{bmatrix} \frac{-R_2R_o}{(R_2+R_o)L} & 0 & \frac{-R_o}{(R_2+R_o)L} \\ 0 & \frac{-1}{R_1C_1} & 0 \\ \frac{R_o}{(R_2+R_o)C_2} & 0 & \frac{-1}{(R_2+R_o)C_2} \end{bmatrix} \quad (10)$$

$$B_{OFF}=\begin{bmatrix} \frac{1}{L} & \frac{-R_2R_o}{(R_2+R_o)L} \\ \frac{1}{R_1C_1} & 0 \\ 0 & \frac{R_o}{(R_2+R_o)C_2} \end{bmatrix} \quad (11)$$

$$C_{OFF}=\begin{bmatrix} \frac{R_2R_o}{R_2+R_o} & 0 & \frac{R_o}{R_2+R_o} \end{bmatrix} \quad (12)$$

$$E=\begin{bmatrix} 0 & \frac{R_2R_o}{R_o+R_2} \end{bmatrix} \quad (13)$$

The time averaging is performed as:

$$\dot{\mathbf{x}}=\left[D\mathbf{A_{ON}}+(1-D)\mathbf{A_{OFF}}\right]+\left[D\mathbf{B_{ON}}+(1-D)\mathbf{B_{OFF}}\right]\mathbf{u} \quad (14)$$

The second step is the adding of small perturbations to the duty-cycle and to all the system states, as follows:

$$\mathbf{x}=\mathbf{X}+\hat{\mathbf{x}}, \quad \text{For } \hat{\mathbf{x}}\ll\mathbf{X} \quad (15)$$

$$D=D+\hat{d}, \quad \text{For } \hat{d}\ll D \quad (16)$$

$$v_{in}=v_{in}+\hat{v}_{in}, \quad \text{For } \hat{v}_{in}\ll v_{in} \quad (17)$$

$$i_o=i_o+\hat{i}_o, \quad \text{For } \hat{i}_o\ll i_o \quad (18)$$

The next step is removing the DC components and also the products of the small signal terms. This step yields the following system of equations:

$$\begin{cases} \dot{\hat{\mathbf{x}}}=\mathbf{A}\hat{\mathbf{x}}+\mathbf{B}'\hat{\mathbf{u}}' \\ \hat{y}=C\hat{\mathbf{x}}+E'\hat{\mathbf{u}}' \end{cases} \quad (19)$$

Where:

$$\mathbf{A}=D\mathbf{A_{ON}}+D'\mathbf{A_{OFF}} \quad (20)$$

$$\mathbf{B}=D\mathbf{B_{ON}}+D'\mathbf{B_{OFF}} \quad (21)$$

$$C=DC_{ON}+(1-D)C_{OFF} \quad (22)$$

$$E=DE_{ON}+(1-D)E_{OFF} \quad (23)$$

$$\mathbf{B_d}=\left[(\mathbf{A_{ON}}-\mathbf{A_{OFF}})\right]\mathbf{X}+\left[(\mathbf{B_{ON}}-\mathbf{B_{OFF}})\right]\mathbf{U} \quad (24)$$

$$\therefore \mathbf{B}'=\begin{bmatrix}\mathbf{B_d} & \mathbf{B}\end{bmatrix} \quad (25)$$

$$E'=\begin{bmatrix}0 & E\end{bmatrix} \quad (26)$$

$$\hat{\mathbf{u}}'=\begin{bmatrix}\hat{d} \\ \hat{\mathbf{u}}\end{bmatrix} \quad (27)$$

Substituting (1) and (2) into (8) results in:

$$A=\begin{bmatrix} \frac{(D-1)R_2R_o}{(R_2+R_o)L} & 0 & \frac{(D-1)R_o}{(R_2+R_o)L} \\ 0 & \frac{-1}{R_1C_1} & 0 \\ \frac{(1-D)R_o}{(R_2+R_o)C_2} & 0 & \frac{-1}{(R_2+R_o)C_2} \end{bmatrix} \quad (28)$$

$$B'=\begin{bmatrix} \frac{R_2R_o}{(R_2+R_o)L}I_L+\frac{R_o}{(R_2+R_o)L}V_{c2} & \frac{1}{L} & \frac{(D-1)R_2R_o}{(R_2+R_o)L} \\ 0 & \frac{1}{R_1C_1} & 0 \\ \frac{-R_o}{(R_2+R_o)C_2}I_L & 0 & \frac{R_o}{(R_2+R_o)C_2} \end{bmatrix} \quad (29)$$

$$C=\begin{bmatrix} \frac{(1-D)R_2R_o}{R_2+R_o} & 0 & \frac{R_o}{R_2+R_o} \end{bmatrix} \quad (30)$$

$$E'=\begin{bmatrix} 0 & 0 & \frac{R_2R_o}{R_2+R_o} \end{bmatrix} \quad (31)$$

2.2. Modeling of the CMC Converter

Among the many available models, the new continuous time model (NCT) in [11, 25] is generally accepted due its simplicity and accuracy. The block diagram of NCT model is represented in Fig. 3, where $\hat{v}_{in}$, $\hat{v}_o$, $\hat{i}_L$ and $\hat{d}$ are the perturbation of the input voltage, output voltage, inductor current, and the duly-cycle of the power stage, respectively. The variable $\hat{v}_c$ is the perturbation of the reference voltage

of the current loop. In this study, $\hat{v}_c$ is the LQR controller output. R_i is the effective linear gain from the sensed current to the comparator input. k_f and k_r are the feedforward and feedback gains, and they are different for the different types of converters. $H_e(s)$ is the sampling gain which is used to model the sampling action in the current loop, for controller design purpose it is taken as a unity.

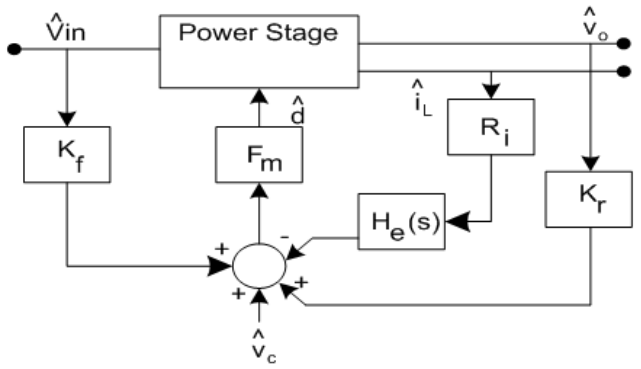

Fig. 3. Small-Signal Model for PCMC Converter.

Modulator gain F_m is the ac gain from the error current signal to the duty-cycle. F_m , k_f and k_r can be expressed as:

$$F_m = \frac{1}{(M_1 + M_c)T_s} \tag{32}$$

$$k_f = \frac{-T_s R_i}{2L} \tag{33}$$

$$k_r = \frac{-D'^2 T_s R_i}{2L} \tag{34}$$

Where M_1 is the positive slope of the inductor current, M_c is the slope of the artificial ramp signal that used for slope compensation. It is stated in [26] that there is an inherent stability when $D > 0.5$ for all the types of the converters. In order to guarantee the controller stability for all range of the duty-cycle, an artificial ramp with slope $M_c \geq 0.5M_2$ has to be added. T_s is the switching period. As it is very small, the k_r can be neglected.

From Fig. 3, when k_r is neglected, the duty ratio law can be expressed as:

$$\hat{d} = F_m(-R_i\hat{i}_L + k_f\hat{v}_g + \hat{v}_c) \tag{35}$$

The state space representation for the small signal analysis can be obtained by replacing the term $\hat{d}$ in (19) with its value in (35). The closed loop matrices are:

$$\mathbf{A} = \begin{bmatrix} \frac{(D-1)R_2R_o - F_mR_iR_o(R_2I_L + V_o)}{(R_2+R_o)L} & 0 & \frac{(D-1)R_o}{(R_2+R_o)L} \\ 0 & \frac{-1}{R_1C_1} & 0 \\ \frac{(1-D)R_o + F_mR_iR_oI_L}{(R_2+R_o)C_2} & 0 & \frac{-1}{(R_2+R_o)C_2} \end{bmatrix} \tag{36}$$

$$\mathbf{B}' = \begin{bmatrix} \frac{F_m(R_oR_2I_L + R_oV_o)}{(R_2+R_o)L} & \frac{(R_2+R_o)+F_mK_fR_o(R_2I_L+V_o)}{(R_2+R_o)L} & \frac{(D-1)R_2R_o}{(R_2+R_o)L} \\ 0 & \frac{1}{R_1C_1} & 0 \\ \frac{-F_mR_o}{(R_2+R_o)C_2}I_L & \frac{-F_mK_fR_oI_L}{(R_2+R_o)C_2} & \frac{R_o}{(R_2+R_o)C_2} \end{bmatrix} \tag{37}$$

$$\mathbf{C} = \begin{bmatrix} \frac{R_1 - R_iF_m}{R_1} & \frac{-1}{R_1} & 0 \end{bmatrix} \tag{38}$$

$$E' = \begin{bmatrix} \frac{F_m}{R_1} & \frac{K_fF_m}{R_1} & 0 \end{bmatrix} \tag{39}$$

3. The Linear Quadratic Regulator –Current Mode Controlled Model

In this section, the optimal control method is applied to the DC-DC boost converter. The controller is formulated as a LQR and the associated cost function is minimized through changes in the control signal of a CMC model.

The design for the compensator gain under optimal control methodology follows from the solution of the state-space matrix **K**. New feedback paths of $\hat{i}_L$, $\hat{v}_{c1}$ and $\hat{v}_{c2}$ are constructed in addition to the existing paths (in the PCMC) as shown in Fig. 4. The linear feedback control is expected to improve the dynamic performance of PCMC PWM converter.

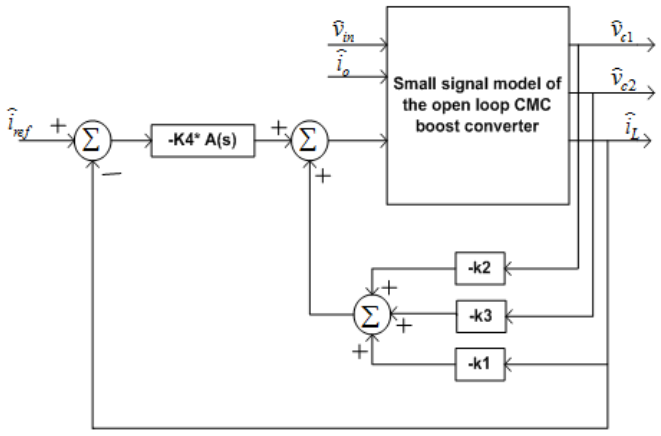

Fig. 4. Small signal model of closed loop CMC PWM boost converter with linear feedback control.

For the averaged model of a boost converter, the linear feedback control law can be written as,

$$\hat{u} = -k_1\hat{i}_L - k_2\hat{v}_{c1} - k_3\hat{v}_{c2} \tag{40}$$

To minimize the steady-state error of the control variable, an integral feedback, $A(s) = 1/s$, is added to the controller. Therefore, a new state variable, $\hat{x}_3 = \hat{\xi}$ is included.

$$\dot{\xi} = i_{ref} - i_{in} = -\mathbf{C}_{1\times3}\begin{bmatrix} i_L \\ v_{c1} \\ v_{c2} \end{bmatrix} - \mathbf{E}'_{1\times3}\begin{bmatrix} v_c \\ v_{in} \\ i_o \end{bmatrix} + i_{ref} \tag{41}$$

$$\dot{\hat{\mathbf{x}}}_{\mathbf{a}} = \underbrace{\begin{bmatrix} \mathbf{A}_{3\times3} & \mathbf{0}_{3\times1} \\ -\mathbf{C}_{3\times1} & \mathbf{0}_{1\times1} \end{bmatrix}}_{\mathbf{A}a}\begin{bmatrix} \hat{\mathbf{x}} \\ \hat{\xi} \end{bmatrix} + \begin{bmatrix} B'_{3\times3} & 0_{3\times1} \\ -E'_{3\times1} & 1 \end{bmatrix}\begin{bmatrix} \hat{u} \\ \hat{i}_{ref} \end{bmatrix} \tag{42}$$

To design the LQR system, the formulation of the following cost function is considered

$$J = \int_0^{+\infty} (\hat{\mathbf{x}}_a{}^T \mathbf{Q}\hat{\mathbf{x}}_{\mathbf{a}} + \rho\hat{V}_c{}^2)dt \tag{43}$$

where $\mathbf{Q}$ is a 4×4 symmetric positive definite matrix, and ρ is a positive scalar. Once $\mathbf{Q}$ and ρ are chosen, the optimal control [17] problem reduces to finding the weights in the vector $\mathbf{K}$ that minimizes (43).

The choice of the matrix $\mathbf{Q}$ and the scalar quantity ρ is very important in the optimization, and both strongly affect the positions of the closed-loop poles. The matrix $\mathbf{Q}$ is chosen to be:

$$\mathbf{Q} = \begin{bmatrix} \mathbf{I}_{3\times3} & \mathbf{0}_{1\times3} \\ \mathbf{0}_{1\times1} & q \end{bmatrix} \tag{44}$$

4. Simulation Results And Discussions

The simulation results of this section are generated using MATLAB/Simulink. The simulated system diagram is shown in Fig. 5(a), where a boost converter is represented by its average circuit [27] , shown in Fig. 5(b), and the LQR-PCMC is modeled as shown in Fig. 5(c). The parameters of the simulated boost circuit are defined as:

$$L = 0.2\text{mH}, C_1 = 50\mu\text{F}, C_2 = 100\mu\text{F}, f = 20\text{kHz},$$
$$R_1 = R_2 = 1\text{m}\Omega, V_{in} = 55\text{V}, V_o = 100\text{V}, I_{in} = 9.1\text{A}.$$

After numerous simulations, the estimated best values for q and ρ are 1×10^8 and 0.1 respectively. These values provide good performance of the system in achieving smooth and short transient responses as shown in the following figures. The resulted gain vector is:

$$\mathbf{K} = \begin{bmatrix} 4.6022 & -1.5811 & -8.49\times10^{-2} & -3.162\times10^4 \end{bmatrix}.$$

In the renewable energy conversion systems, the boost input current is variable according to the reference current generated by MPPT algorithms. In addition, the input voltage is not constant as it is affected by the renewable source conditions. In the wind energy conversion system, for example, the input voltage of the boost is a function of the output voltage of the generator which relates to the generator speed. The generator speed should change instantaneously to maintain its ratio with the wind speed at the optimal value. Therefore, the input voltage is also considered variable. Moreover, the output voltage of the boost converter is the voltage of the dc bus, which is regulated using a storage element connected by another dc-dc converter. Thus, it suffers enormously from the transient conditions, which acts like a disturbance for the boost converter.

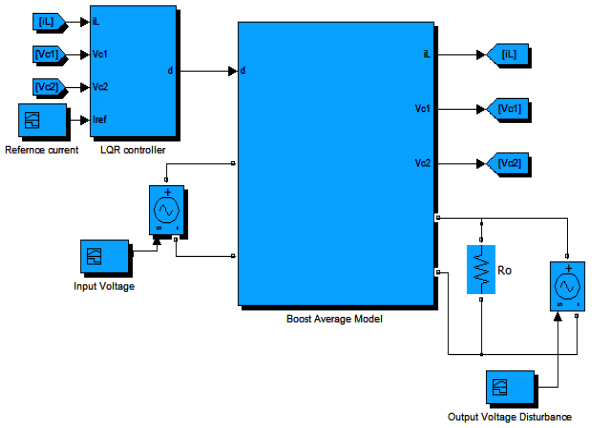

(a)

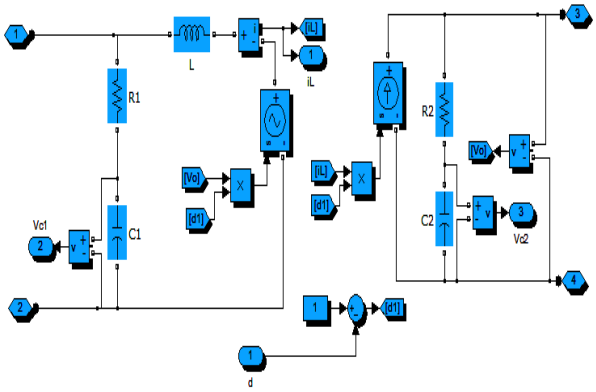

(b)

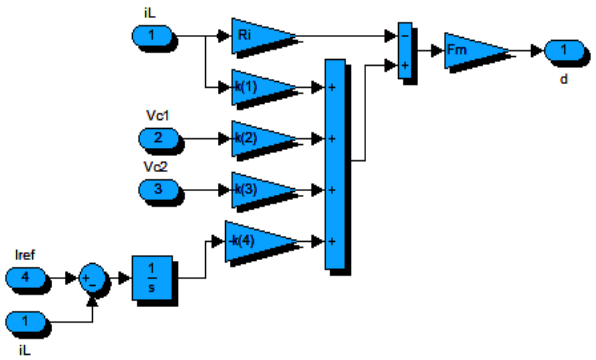

(c)

Fig. 5. (a) The simulated system diagram (b) The boost average model subsystem (c) The LQR controller subsystem.

For $q = 1\times10^{8}$ and $\rho = 0.1$, the closed-loop boost converter is tested under three different disturbance signals. The first case is a step change on the reference input current from 9.1 A to 10 A and then to 8 A. From Fig. 6, it can be clearly seen that the inductor current tracks the change in the reference current correctly with slight transients. Where the inductor current settles at the start-up in approximately 64μs with 0.95% overshoot, it also tracks the change that occurred at 0.01s and 0.02 s very softly in 0.619ms and 0.1ms, respectively.

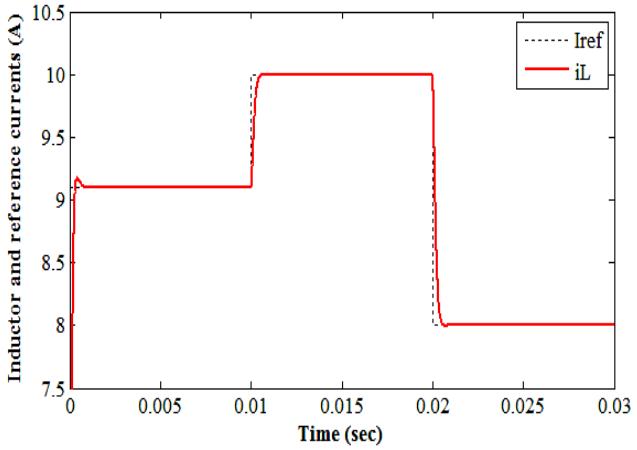

Fig. 6. Inductor current response to a step input current variations from 9.1 A to 10 A and then to 8 A.

A good dynamic behaviour is also depicted in Fig. 7 after a step change on the output voltage. For a 10 V step change in the output voltage, the peak undershoot in the inductor current is 8.42% and the recovery time is 0.84 ms. They are also 1.88A and 1.13 ms for a 20V step change.

As a final case, a step variation in the input voltage by 10 V and 15 V is done, as shown in Fig. 8. Although the initial inductor current changes by about 32.4%, it recovers its nominal value in less than 0.9 ms. The next change is recovered in less than 1.17 ms with almost 3.81A inductor current change.

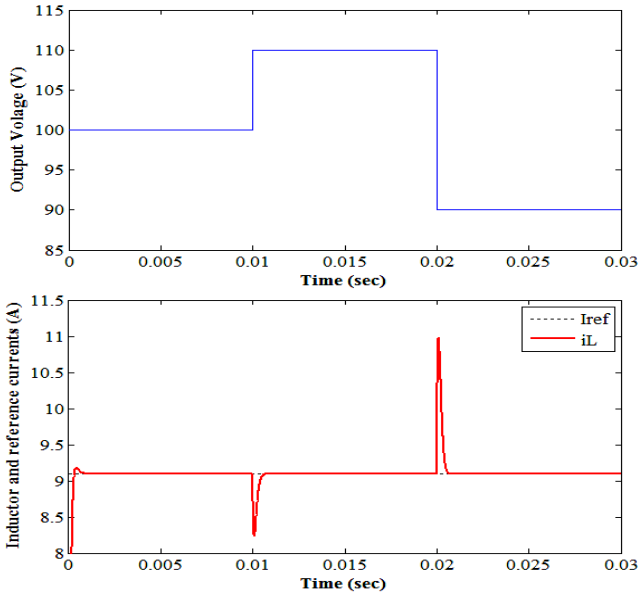

Fig. 7. Inductor current response to a step output voltage variations from 100V to 110V and then to 90V.

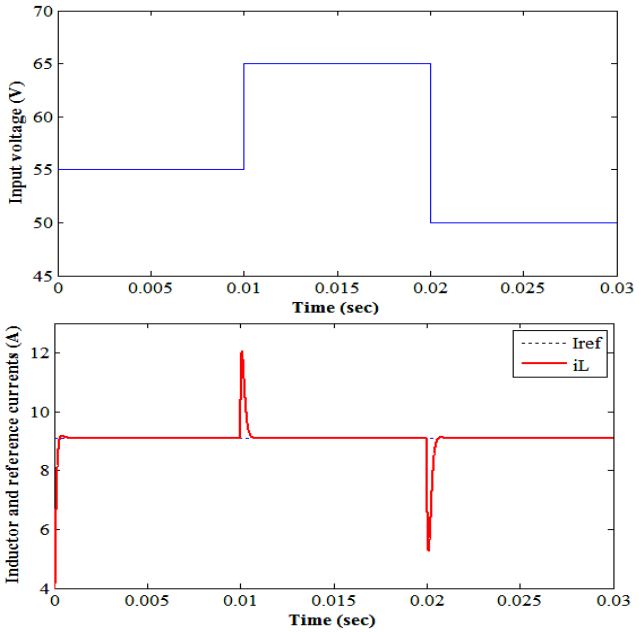

Fig. 8. Inductor current response to a step input voltage variations from 55V to 65V and then to 50V.

5. Conclusion

Changing the input current of the boost converter to absorb the maximum power from the renewable energy sources is accompanied with a change in the input and output voltages due to different reasons. Therefore, the controller to be used should be robust and able to reject these disturbances. Although, the derived models are for the small signal variations, and the weighting matrices of the LQR method are not the optimal. Nevertheless, the LQR-CMC controller that proposed in this paper is successfully achieved the desired performance that is fast with accepted overshoots and undershoots. Moreover, it can recover the system to its nominal operating point upon being exposed to the disturbance in a very short time. Applying this controller to the renewable-energy sources whose MPPT algorithms depend on the input current of the converter surely will make it more efficient.

References

[1] Abdullah MA, Yatim AHM, Chee Wei T. A study of maximum power point tracking algorithms for wind energy system. 2011 IEEE First Conference on Clean Energy and Technology (CET), 2011. p. 321-6.

[2] Muhtaroglu A. A novel digital MPPT control architecture for renewable system integration. 2010 IEEE International Conference on Sustainable Energy Technologies (ICSET), 2010. p. 1-4.

[3] Brunton SL, Rowley CW, Kulkarni SR, Clarkson C. Maximum power point tracking for photovoltaic optimization using ripple-based extremum seeking control. IEEE Transactions on Power Electronics, 2010;25:2531-40.

[4] Esram T, Chapman PL. Comparison of photovoltaic array maximum power point tracking techniques. IEEE Transactions on Energy Conversion. 2007;22:439-49.

[5] Abdullah MA, Yatim AHM, Tan CW, Saidurb R. A review of maximum power point tracking algorithms for wind energy systems. Renewable and Sustainable Energy Reviews, vol. 16, pp. 3220-3227, 2012.

[6] Neammanee B, Sirisumranukul S, Chatratana S. Control performance analysis of feedforward and maximum peak power tracking for small-and medium-sized fixed pitch wind turbines. '06 9th International Conference on Control, Automation, Robotics and Vision, 2006 ICARCV, 2006. p. 1-7.

[7] Kesraoui M, Korichi N, Belkadi A. Maximum power point tracker of wind energy conversion system. Renewable Energy. 2011;36:2655-62.

[8] Patsios C, Chaniotis A, Rotas M, Kladas AG. A comparison of maximum-power-point tracking control techniques for low-power variable-speed wind generators. 8th International Symposium on Advanced Electromechanical Motion Systems & Electric Drives Joint Symposium, 2009. p. 1-6.

[9] Hua ACC, Cheng BCH. Design and implementation of power converters for wind energy conversion system. International Power Electronics Conference (IPEC), 2010. p. 323-8.

[10] Koutroulis E, Kalaitzakis K. Design of a maximum power tracking system for wind-energy-conversion applications. IEEE Transactions on Industrial Electronics. 2006;53:486-94.

[11] Ridley RB. A new, continuous-time model for current-mode control [power convertors]. IEEE Transactions on Power Electronics,. 1991;6:271-80.

[12] Tang W, Lee FC, Ridley RB. Small-signal modeling of average current-mode control. IEEE Transactions on Power Electronics,. 1993;8:112-9.

[13] Midya P, Krein PT, Greuel MF. Sensorless current mode control-an observer-based technique for. IEEE Transactions on Power Electronics,. 2001;16:522-6.

[14] Anderson BDO, Moore JB. Optimal Control, Linear Quadratic Methods: Prentice Hall; 1990.

[15] Liu H, Mao C, Lu J, Wang D. Optimal regulator-based control of electronic power transformer for distribution systems. Electric Power Systems Research. 2009; 79:863-70.

[16] Jaen C, Pou J, Pindado R, Sala V, Zaragoza J. A linear-quadratic regulator with integral action applied to pwm dc-dc converters. IEEE Industrial Electronics, IECON 2006 - 2006. p. 2280-5.

[17] Dores Costa JM. Design of linear quadratic regulators for quasi-resonant DC-DC converters. Power Electronics Specialists Conference, 2001 PESC 2001 IEEE 32nd Annual2001. p. 422-6 vol. 1.

[18] Beccuti AG, Papafotiou G, Morari M. Optimal control of the buck dc-dc converter operating in both the continuous and discontinuous conduction regimes. 45th IEEE Conference on decision and control, 2006. p. 6205-10.

[19] Beccuti AG, Papafotiou G, Morari M. Optimal control of the boost dc-dc converter. European Control Conference CDC-ECC '05 and 44th IEEE Conference on Decision and Control,2005. p. 4457-62.

[20] Gezgin C, Heck BS, Bass RM. Control structure optimization of a boost converter: an LQR approach. Power Electronics Specialists Conference, 1997 PESC '97 Record, 28th Annual IEEE1997. p. 901-7 vol.2.

[21] Nejati R, Eshtehardiha S, Poudeh MB. Improvement of step-down converter performance with optimum LQR and PID controller with applied genetic algorithm. AIP Conference Proceedings. 2008; 1052:129-34.

[22] Mahdavian M, Poudeh MB, Eshtehardiha S. DC-DC converter with closed loop control through several optimizing methods. nternational Conference on Optimization of Electrical and Electronic Equipment, 2008 OPTIM, 2008. p. 233-8.

[23] Hasaneen BM, Elbaset Mohammed AA. Design and simulation of DC/DC boost converter. 12th International Middle-East Power System Conference, MEPCON , 2008. p. 335-40.

[24] B J. Improved models for DC-DC converters. Sweden: Lund University; 2003.

[25] Al-Mothafar MRD, Hammad KA. Small-signal modelling of peak current-mode controlled buck-derived circuits. IEE Proceedings - Electric Power Applications. 1999; 146:607-19.

[26] Mitchell DM. Dc-Dc Switching Regulator Analysis: Mcgraw-Hill (Tx) 1998.

[27] Al-Mothafar MRD. Small- and large-signal modelling of a modular boost-derived DC-DC converter for high-output voltage applications. Int J Model Simul. 2006; 26:52-60.